

LETTER TO THE EDITOR

OGLE GD-CEP-0516: the most metal-poor lithium-rich Galactic Cepheid.[★]

G. Catanzaro¹, V. Ripepi², M. Salaris^{3,4}, and E. Trentin^{5,6,2}

¹ INAF-Osservatorio Astrofisico di Catania, Via S.Sofia 78, 95123, Catania, Italy
e-mail: giovanni.catanzaro@inaf.it

² INAF-Osservatorio Astronomico di Capodimonte, Salita Moiariello 16, 80131, Naples, Italy
e-mail: vincenzo.ripepi@inaf.it

³ Astrophysics Research Institute, Liverpool John Moores University, 146 Brownlow Hill, Liverpool L3 5RF, UK
e-mail: m.salaris@ljmu.ac.uk

⁴ INAF - Osservatorio Astronomico di Abruzzo, Via M. Maggini, s/n, I-64100 Teramo, Italy

⁵ Leibniz-Institut für Astrophysik Potsdam (AIP), An der Sternwarte 16, D-14482 Potsdam, Germany
e-mail: etrentin@aip.de

⁶ Institut für Physik und Astronomie, Universität Potsdam, Haus 28, Karl-Liebknecht-Str. 24/25, D-14476 Golm (Potsdam), Germany

ABSTRACT

Context. Classical Cepheids (DCEPs) are important astrophysical objects not only as standard candles for the determination of the cosmic distance ladder but also as a test-bed for the stellar evolution theory, thanks to the connection between their pulsation (periods, amplitudes) and stellar (luminosity, mass, effective temperature, metallicity) parameters.

Aims. We aim at unveiling the nature of the Galactic DCEP OGLE-GD-CEP-0516 and other DCEPs showing enhanced abundance of lithium in their atmospheres.

Methods. We have collected high-resolution spectrum for OGLE-GD-CEP-0516 with UVES@VLT. Accurate stellar parameters: effective temperature, gravity, micro- and macro-turbulence, radial velocity, and metal abundances were measured for this star, by using spectral synthesis techniques based on LTE plane-parallel atmospheric model.

Results. We measured a chemical pattern with most elements under-abundant compared with the Sun, i.e. $[\text{Fe}/\text{H}] = -0.54 \pm 0.16$ dex, $[\text{C}/\text{H}] = -0.45 \pm 0.05$ dex, or $[\text{Mg}/\text{H}] = -0.40 \pm 0.16$ dex among others. In particular, we measured a lithium abundance $A(\text{Li}) = 3.06 \pm 0.10$ dex for OGLE-GD-CEP-0516, which makes this object the sixth Li-rich object among the Milky Way DCEPs.

Conclusions. Our results favour the scenario in which the six Galactic Li-rich DCEPs are first-crossing the instability strip having had slowly-rotating progenitors during their main sequence phase. This study explored the link between lithium abundance and the pulsation period in classical Cepheids. It found that brighter Cepheids, indicative of higher mass, show enhanced lithium abundance, contrary to predictions from evolutionary models considering rotation. Additionally, an analysis of lithium abundance versus $[\text{Fe}/\text{H}]$ revealed a lack of significant correlation, contradicting expectations from galactic chemical evolution (GCE) models.

Key words. Stars: variables: Cepheids – Stars: abundances – Stars: fundamental parameters – Stars: individual: OGLE-GD-CEP-0516

1. Introduction

Classical Cepheids (DCEPs) are the most important standard candle for the extragalactic distance scale and are powerful tracers of the young (~ 50 – 300 Myr) populations inside a galaxy, including the Milky Way. Moreover, observations of DCEPs are also crucial to further our understanding of the physical mechanisms governing their evolution and pulsation. In this context, the rare lithium-rich DCEPs subclass is of particular interest. Indeed, only five DCEPs showing enhanced lithium abundance (through the detection of the $\text{LiI } 6707.766 \text{ \AA}$) have been discovered in the Galaxy so far (Luck & Lambert 2011; Kovtyukh et al. 2016, 2019; Catanzaro et al. 2020) and an additional one was detected in the Large Magellanic Cloud (LMC, Luck & Lambert 1992). All these objects show a surface lithium abundance $A(\text{Li}) \sim 3.0$ dex, in contrast to the majority of the Galactic

DCEPs, which show $A(\text{Li}) < 1.2$ dex (Luck & Lambert 2011). This discovery was surprising, as Li is expected to be depleted by proton-capture after the first dredge-up (1DU) occurring at the beginning of the Red Giant Branch (RGB) phase (Iben 1967). A natural explanation is that these DCEPs are at their first crossing of the IS and their envelopes do not show the signature of nuclear processes that occurred during the Main Sequence (MS) phase. Indeed, according to Kovtyukh et al. (2019), at least three of the four Milky Way (MW) Li-rich DCEPs also show abundances of the CNO species which are consistent with the solar values, i.e. not processed by the CN-cycle. However, the 1DU is not the only phenomenon capable of depleting lithium. Rotational mixing can reduce the lithium abundance by a factor of a hundred in a fraction of the MS lifetime, for sufficiently fast rotating MS stars (e.g. Brott et al. 2011). This would then explain the scant number of Li-rich DCEPs. Indeed, as noted by Kovtyukh et al. (2019), about 80% of the DCEPs expected to be at their first crossing (about 5% of the total) are Li-depleted.

[★] Based on observations European Southern Observatory programs P105.20MX.001

Table 1. Main characteristics of OGLE-GD-CEP-0516.

<i>Gaia</i> DR3 ID	P	Mode	G	A_V
	days		mag	mag
5255256669866274816	0.394959	1O/2O	12.462	1.446 ^a

Notes. a = Anders et al. (2019)

Therefore it can be hypothesized that the progenitors of the Li-rich and Li-depleted DCEPs (B stars) were, respectively, slow and fast rotators during their MS evolution. It is known that a fraction ($\sim 15\%$) of the B-stars show $v \sin i < 20 \text{ km s}^{-1}$ (Huang et al. 2010), while the large majority rotates much faster. It is thought that the slow rotators lose most of their angular momentum on the MS due to stellar winds enhanced by the rotation itself (Maeder & Meynet 2000). Therefore, upon becoming DCEPs they show the moderate rotational velocities typical of these stars.

An additional feature of the Li-rich DCEPs is that they most frequently are multi-mode pulsators. Among the five MW Li-rich DCEPs, ASAS J075842-2536.1, ASAS J131714-6605.0 and V363 Cas pulsate in the first and second overtone (DCEP_1O2O), V371 Per pulsates in the fundamental and first overtone (DCEP_F1O), whereas V1033 Cyg is only a fundamental mode (DCEP_F) pulsator. According to Kovtyukh et al. (2019), multi-mode DCEPs have a less efficient mixing in their envelope than DCEP_F, hence would preferentially tend to retain their Li.

Even if other more complex processes can address the presence of lithium in DCEPs (see Kovtyukh et al. 2019, for a detailed discussion), the basic mechanism to explain Li-rich DCEPs is their transit through the IS at the first crossing. This occurrence can be verified by measuring the rate of period change due to their evolution along the Hertzsprung-Russell Diagram (HRD), as the period is expected to increase at the first and third crossing, and decrease at the second one (see e.g. Turner et al. 2006). The data available allowed Kovtyukh et al. (2019) to detect a quick period change in V1033 Cyg and Catanzaro et al. (2020) in V363 Cas whereas they were insufficient to detect period changes in the other three MW DCEPs.

In the course of a large project devoted to measuring the metallicity dependence of DCEPs period-luminosity relations dubbed C-MetaLL¹ (Cepheid - Metallicity in the Leavitt Law, see Ripepi et al. 2021; Trentin et al. 2022), we obtained high-resolution spectroscopy for hundreds of Galactic DCEPs. As a by-product of the C-MetaLL projects, we searched systematically all the targets for the presence of a deep Li I 6707.766 Å line in their spectra. In this letter, we report the successful detection of a such lithium line in the Galactic DCEP OGLE-GD-CEP-0516.

2. Spectroscopic observations and data analysis

We collected high-resolution spectroscopy for OGLE-GD-CEP-0516 using the Ultraviolet and Visual Echelle Spectrograph (UVES)² instrument, operated by the European Southern Observatory (ESO) and attached to the Unit Telescope 2 of the Very Large Telescope (VLT), placed at Paranal (Chile). The spectrum covers the wavelength range between $\lambda\lambda$ 4790 to 6800 Å, with a spectral resolution $R=47\,000$. The signal-to-noise ratio (SNR)

varies from 80 to 100. The main characteristics of OGLE-GD-CEP-0516 are summarised in Table 1.

The spectrum reduction, which included bias subtraction, spectrum extraction, flat fielding, and wavelength calibration, was performed using the ESO reduction pipeline. The radial velocity was measured by cross-correlating the observed spectrum with a synthetic template, using the Image Reduction and Analysis Facility (IRAF) task FXCOR and excluding Balmer lines as well as wavelength ranges containing telluric lines. The IRAF package RVCORRECT was adopted to determine the heliocentric velocity by correcting the spectrum for the Earth's motion.

All the important quantities characterizing the stellar atmosphere, such as effective temperature (T_{eff}), surface gravity ($\log g$), microturbulent (ξ), and lines broadening contributions (v_{br}) due to the combined effects of $v \sin i$ and macroturbulent velocity (that is a dominant contribution in DCEP), have been already derived in Trentin et al. (2022). These quantities are listed in Table 2.

As a check of these parameters (principally T_{eff} and $\log g$), we reproduced the observed spectral energy distribution (SED) with the synthetic flux computed using the plane parallel local thermodynamic equilibrium (LTE) atmosphere models computed using the ATLAS9 code (Kurucz 1993). The observed flux was retrieved from the Virtual Observatory SED Analyzer (VOSA Bayo et al. 2008) and corrected for reddening adopting $A_V = 1.446$ mag (Anders et al. 2019) and the Fitzpatrick (1999) extinction law. The comparison between the observed and the theoretical SEDs is satisfactory, as shown in Fig. A.1. The SED can be used to estimate the bolometric luminosity L_{bol} of OGLE GD-CEP-0516, provided we know its distance. To this aim we adopted the distance obtained by Bailer-Jones et al. (2021) based on *Gaia* Early Data Release 3 (EDR3 *Gaia* Collaboration et al. 2016, 2021), obtaining a final value of $L_{\text{bol}} = 140 \pm 5 L_{\odot}$.

As an additional check regarding the line broadening value reported in Trentin et al. (2022), we adopted the code iacob-broad described in Simón-Díaz & Herrero (2014) to disentangle the effects of the rotational velocity to that of macroturbulence. In this code, the authors assumed a radial-tangential definition of the macroturbulence profile (see Gray 2008, for a detailed description). In a few words, we derived the macroturbulent velocity from the goodness-of-fit method (using a χ^2 formalism) when the $v \sin i$ is fixed to the value corresponding to the first zero of the Fast Fourier Transform (FFT) of a chosen line profile. For this calculation, we have chosen five spectral lines well isolated in the spectrum and for which signal-to-noise on both sides of the line is > 150 , namely: Fe I $\lambda\lambda$ 6003.011, 6027.051, 6056.004, 6065.481, and 6252.555 Å. The FFT of those lines is shown with different colors in Fig. A.2. For each of those we computed both $v \sin i$ (first zero of the FFT) and Θ_{RT} (by goodness-of-fit technique), and the weighted means of the results are reported in Table 2. As expected the macroturbulence velocity completely dominates the rotational profile, being consistent with the value of v_{br} given by Trentin et al. (2022).

Except for lithium, the abundances reported in Table A.1 have been calculated by Trentin et al. (2022). Regarding lithium, we proceeded with this target as described in Catanzaro et al. (2020), i.e. by a spectral synthesis performed using code (SYN-THE Kurucz & Avrett 1981) applied to an LTE plane-parallel atmosphere model computed by ATLAS9 (Kurucz 1993) for T_{eff} and $\log g$ reported in Table 2. According to Amarsi et al. (2020) the non-LTE departure for [Li/H] in giant stars with the metallicity of our target, is ≈ 0.05 dex, negligible for this study. In Fig. 1 we show the comparison between observed and synthetic spec-

¹ <https://sites.google.com/inaf.it/c-metall/home>

² <https://www.eso.org/sci/facilities/paranal/instruments/uves.html>

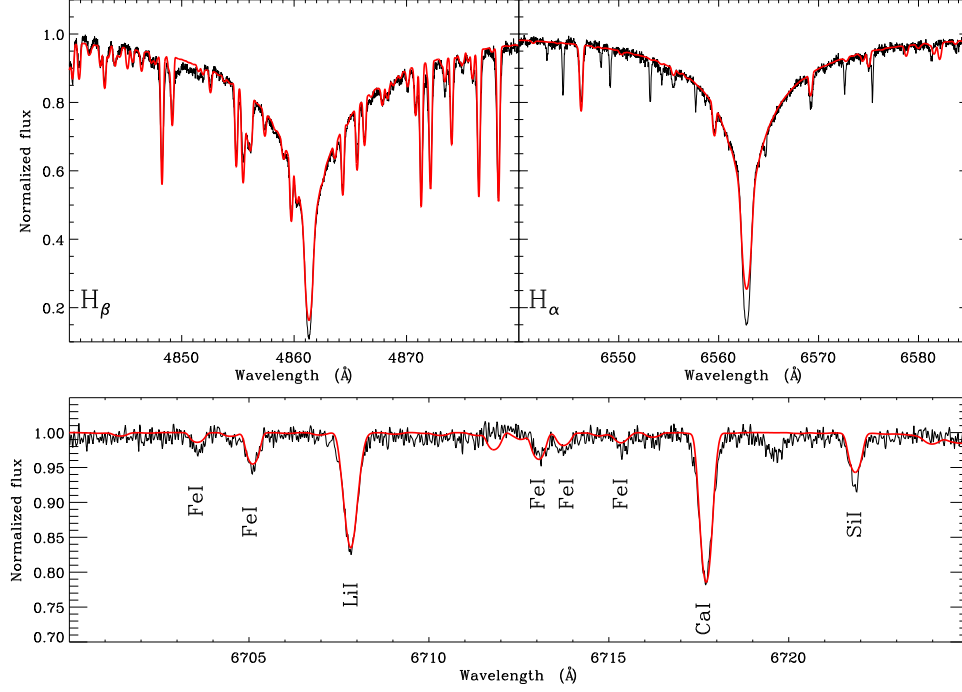


Fig. 1. Comparison between the spectrum of OGLE-GD-CEP-0516 obtained (black line) and the synthetic spectrum (red line) in three main spectral intervals centred, respectively, on $H\beta$ (top-left panel), $H\alpha$ (top-right panel) and the Li I line at 6707.766 \AA (bottom panel). The spectral features not reproduced with synthetic spectrum in the wing of $H\alpha$ are telluric lines. The lithium line has been reproduced with $A(\text{Li}) = 3.06 \pm 0.10 \text{ dex}$.

Table 2. Atmospheric parameters adopted for OGLE-GD-CEP-0516. We list adopted effective temperature, gravity, microturbulence, line broadening, projected rotational velocity, radial-tangential macroturbulence, heliocentric Julian day of the middle exposure, and radial velocities.

T_{eff} (K)	$\log g$	ξ (km s^{-1})	v_{br} (km s^{-1})	$v \sin i$ (km s^{-1})	Θ_{RT} (km s^{-1})	HJD (2450000.0+)	v_{rad} (km s^{-1})
6400 ± 150	1.5 ± 0.1	2.4 ± 0.2	13 ± 1	9.2 ± 0.6	12.3 ± 2.4	9217.6507	-9.0 ± 0.2

tra in three main spectral regions, namely, $H\beta$ and $H\alpha$, and the $\text{Li I } 6708.766 \text{ \AA}$ line. For the synthesis of the Li I line, we took into account the hyperfine structure and the close $\text{Fe I } 6708.282 \text{ \AA}$ line. The abundances of all the 24 species we detected in the spectrum of OGLE-GD-CEP-0516 are displayed in Fig. A.3. The analysis of this chemical pattern shows clearly that our target is metal-poor, being the most contributors to the metallicity under-abundant compared with the solar composition (Grevesse et al. 2010). Furthermore, since $[\text{Fe}/\text{H}] = -0.54 \text{ dex}$, we can conclude that OGLE-GD-CEP-0516 is the most metal-poor lithium-rich Galactic Cepheid.

The lithium line was reproduced with an abundance $A(\text{Li}) = 3.06 \pm 0.10$, the error on the lithium abundance was calculated by propagating the errors on the atmospheric parameters, i.e. δT , $\delta \log g$, and $\delta \xi$. This value is greater than the results from the standard Big Bang nucleosynthesis theory, which predicts a lithium abundance of $A(\text{Li}) = 2.72 \pm 0.06 \text{ dex}$ (Cyburt et al. 2008), but it is in agreement with the predictions of the Galactic Chemical Evolution models (GCE, e.g. Romano et al. 2021).

3. Discussion

The luminosity and the effective temperature derived in the previous section for OGLE GD-CEP-0516 allowed us to place the star in the HR diagram. According to the evolutionary tracks by Bressan et al. (2012) its mass is $M \approx 2.7 M_{\odot}$. For comparison pur-

poses, we placed in the same HR diagram all the DCEPs with lithium discovered so far, after a new estimate of their luminosities. In particular, we used the effective temperatures from the original sources, i.e. from Kovtyukh et al. (2019) for all the stars except for V363 Cas taken from Catanzaro et al. (2020), extinctions from Anders et al. (2019) and distances from Bailer-Jones et al. (2021). All these data have been reported in Table 3.

When the DCEPs cross the instability strip for the first time, their surface chemical composition is the same as at the end of the main sequence phase. When the first dredge-up occurs, the surface abundances of the CNO elements change because Li-free material coming from the inner part of the star is mixed into the convective envelope. In particular, carbon becomes deficient relative to its initial abundance by about -0.3 dex , nitrogen is increased by $\sim 0.3 \text{ dex}$, while oxygen should remain practically unchanged (see for example, Lyubimkov et al. 2011, 2015; Adamczak & Lambert 2014). Moreover, another possible evolutionary status indicator is the abundance of Na which appears to be enhanced in post-first dredge-up intermediate-mass stars (Sasselov 1986; Denissenkov 1994; Takeda et al. 2013). The limiting factor in this interpretation is the lack of knowledge of the initial abundance while the star is in the main sequence. In the case of OGLE GD-CEP-0516, we find C, O, and Na underabundant compared to the solar values, but this is not evidence for the first dredge-up because our target exhibits an overall low metallicity. This occurrence reinforces our hypothesis that the star is crossing the instability strip for the first time.

Table 3. Main parameters of the known MW Li-rich DCEPs. Distances are from Bailer-Jones et al. (2021), extinctions from Anders et al. (2019), effective temperatures, lithium and iron abundances are from Kovtyukh et al. (2019) for all the stars except for V363 Cas taken from Catanzaro et al. (2020). Luminosities have been computed by using VOSA tools.

Star	D (pc)	A_V (mag)	T_{eff} (K)	L (L_\odot)	A(Li) (dex)	[Fe/H] (dex)
ASAS J075842-2536.1	2601 ± 115	0.939	6295	145 ± 14	2.84 ± 0.10	-0.16 ± 0.12
ASAS J131714-6605.0	2746 ± 92	1.686	6308	524 ± 35	2.96 ± 0.10	0.05 ± 0.06
V371 Per	3255 ± 129	0.319	5973	474 ± 39	3.09 ± 0.10	-0.46 ± 0.09
V1033 Cyg	3621 ± 374	2.478	5819	911 ± 190	3.18 ± 0.10	0.01 ± 0.11
V363 Cas	1215 ± 16	1.545	6660	287 ± 8	2.86 ± 0.10	-0.30 ± 0.12

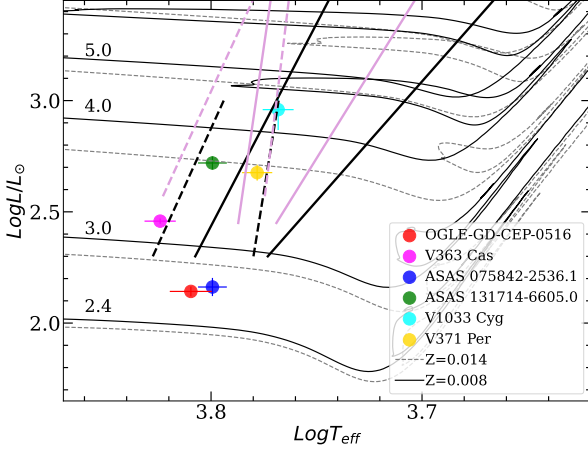


Fig. 2. HR diagram of the known MW Li-rich DCEPs. OGLE GD-CEP-0516 is shown by the filled red circle. Different symbols are used for the other five literature stars (see labels). The Instability strips for fundamental (solid lines) and first overtone (dashed lines) DCEPs by De Somma et al. (2020) as well as evolutionary tracks by Bressan et al. (2012) for $Z = 0.008$ (solid line) and $Z = 0.014$ (grey dashed line) in the mass range $2.4\text{--}5.0 M_\odot$ are also over-plotted on the data.

To further investigate the properties of Li-rich DCEPs, we searched for possible correlations between lithium and iron abundances, and also lithium abundances versus pulsational period. Figure 3 (left panel) displays an A(Li) vs [Fe/H] diagram. The sample of Li-rich DCEPs spans a relatively wide range in metallicity, from solar to [Fe/H] = -0.56 dex. The dispersion of A(Li) values around the mean is approximately 0.13 dex, exceeding the errors in individual measurements. The present sample of Li-rich DCEPs does not show any statistically significant correlation between lithium and iron. This finding is at odds with the predictions of the GCE models by e.g. Romano et al. (2021) which display a significant reduction of the lithium abundance when moving from [Fe/H] ~ 0.0 dex to [Fe/H] ~ -0.5 dex (see their Fig. 6). The right panel of Fig 3 shows the distribution of A(Li) as a function of pulsation periods. We observed a moderate to strong positive Spearman rank correlation coefficient of 0.66 between the variables. However, the associated significance of deviance from zero of 16% indicates that, although the correlation is not statistically significant at the 5% level, there is still a noteworthy relationship. Therefore, further investigation is needed to better understand this result. As the periods of DCEPs increase with the luminosity and, in turn, thanks to the mass-luminosity relation, with the mass, we can conclude that brighter (more massive) objects show larger lithium abundances. To investigate

more in detail this unexpected finding, in Fig. 4, we compare the lithium abundance of the six DCEPs versus T_{eff} with the predictions of the evolutionary models STAREVOL (v3.00) (Lagarde et al. 2012, non-rotating and with thermohaline and rotation-induced mixings). More in detail, by considering models for [Fe/H] = 0.0 dex, we show the evolution of A(Li) versus T_{eff} for two masses, $2.5 M_\odot$ and $4.0 M_\odot$ both with and without rotation. According to Fig 2 these values encompass the range of masses spanned by Li-rich DCEPs. Models without rotation do not predict lithium depletion within our temperature range as mass varies. Conversely, evolutionary models that take rotation into account show a strong lithium depletion of ≈ 1.4 dex and ≈ 1.8 dex, respectively for $2.5 M_\odot$ and $4.0 M_\odot$. According to these models, less massive objects deplete more lithium in their atmosphere if they rotate. These predictions are in contrast to the trend shown by Li-rich DCEPs displayed in the right panel of Fig. 3. Indeed, in the case of no rotation we should not expect any trend of lithium abundance with mass, while in the case of rotation, the expected trend is the opposite of what is observed. This strongly suggests that mixing due to rotation has not critically affected the evolution of the surface Li abundances in these stars, and that the measured A(Li) should closely reflect the initial values. In addition, we have to take into account that the surface rotation velocity in the STAREVOL models is on the order of $80\text{--}90 \text{ km s}^{-1}$, considerably larger than what is measured for these DCEPs whose surface rotation velocity, according to our measures, should not exceed $10\text{--}20 \text{ km s}^{-1}$. This also points to a very small surface Li depletion.

Based on these figures, a possible working scenario able to reconcile theory and observations is to hypothesize that more massive DCEPs rotate at a slightly slower surface velocity than the less massive ones. As lithium depletion is significant for large rotation velocities, we can speculate about the difference in rotational velocity between more and less massive DCEPs that should be at most $\sim 10 \text{ km s}^{-1}$, a value compatible with the typical velocities measured in our targets.

4. Conclusions

In this letter, we reported the discovery of the sixth Li-rich DCEP, OGLE GD-CEP-0516. This object confirms the tendency of these objects to be short-period overtone pulsators. The presence of lithium in DCEP atmospheres is a rare event. In the course of the C-MetaLL project, we obtained spectroscopy for more than 330 DCEPs (e.g. Trentin et al. 2022, and Trentin et al. 2024, in preparation), finding significant lithium abundance only in V363 Cas and OGLE GD-CEP-0516. The high abundance of lithium and the low luminosity of OGLE GD-CEP-0516 require that it cross the IS for the first time and has not experienced the first DU. Considering the ensemble properties of all the six

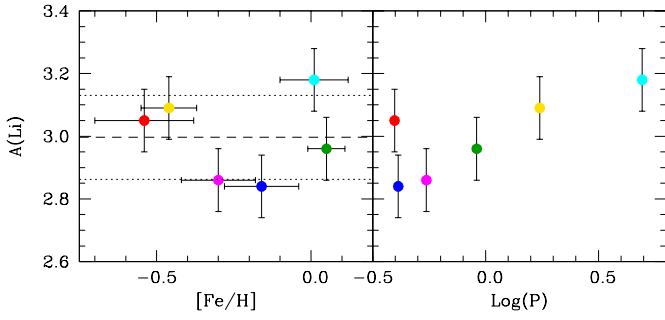


Fig. 3. Lithium abundances versus $[Fe/H]$ and the logarithm of pulsation periods, respectively in the left and right panel. Colours have the same meaning as Fig. 2. In the left panel, the dashed line represents the average $A(Li)$, while dotted lines represent the $\pm 1\sigma$ level.

known Li-rich DCEPs in comparison with stellar evolution and GCE models, we find a general disagreement between theory and observations: i) the DCEPs span a metallicity range between 0.0 dex and -0.56 dex. In this interval, the measured lithium abundance is approximately constant, while GCE models predict a significant decrease to reach the plateau at $A(Li) \sim 2.7$ dex; ii) the Li-rich DCEPs show larger $A(Li)$ values at larger masses (luminosities). According to evolutionary models, this trend might be explained by hypothesizing that higher-mass DCEPs rotate slightly slower than less massive ones.

All the above conclusions are based on a small statistical sample of only six objects. An increase in the number of Li-rich DCEPs is essential to further our understanding of this puzzling phenomenon. To this aim, future wide spectroscopic surveys such as those planned with the WEAVE (WHT Enhanced Area Velocity Explorer)³ and 4MOST (4-metre Multi-Object Spectroscopic Telescope)⁴ may allow us to discover many new Li-rich DCEPs and obtain new insight to obtain a definitive explanation for their existence.

Acknowledgements. We thank our anonymous Referee for her/his helpful comments. This work has made use of data from the European Space Agency (ESA) mission *Gaia* (<https://www.cosmos.esa.int/gaia>), processed by the *Gaia* Data Processing and Analysis Consortium (DPAC, <https://www.cosmos.esa.int/web/gaia/dpac/consortium>). Funding for the DPAC has been provided by national institutions, in particular, the institutions participating in the *Gaia* Multilateral Agreement. This publication makes use of VOSA, developed under the Spanish Virtual Observatory project supported by the Spanish MINECO through grant AyA2017-84089. VOSA has been partially updated by using funding from the European Union’s Horizon 2020 Research and Innovation Programme, under Grant Agreement n° 776403 (EXOPLANETS-A). This research has made use of the SIMBAD database, operated at CDS, Strasbourg, France.

References

Adamczak, J. & Lambert, D. L. 2014, *ApJ*, 791, 58
 Amarsi, A. M., Lind, K., Osorio, Y., et al. 2020, *A&A*, 642, A62
 Anders, F., Khalatyan, A., Chiappini, C., et al. 2019, *A&A*, 628, A94
 Bailer-Jones, C. A. L., Rybizki, J., Fousneau, M., Demleitner, M., & Andrae, R. 2021, *AJ*, 161, 147
 Bayo, A., Rodrigo, C., Barrado Y Navascués, D., et al. 2008, *A&A*, 492, 277
 Bressan, A., Marigo, P., Girardi, L., et al. 2012, *MNRAS*, 427, 127
 Brott, I., de Mink, S. E., Cantiello, M., et al. 2011, *A&A*, 530, A115
 Catanzaro, G., Ripepi, V., Clementini, G., et al. 2020, *A&A*, 639, L4
 Cyburt, R. H., Fields, B. D., & Olive, K. A. 2008, *J. Cosmology Astropart. Phys.*, 2008, 012
 De Somma, G., Marconi, M., Molinaro, R., et al. 2020, *ApJS*, 247, 30

³ <https://www.ing.iac.es/astronomy/instruments/weave/weaveinst.html>

⁴ <https://www.eso.org/sci/facilities/develop/instruments/4MOST.html>

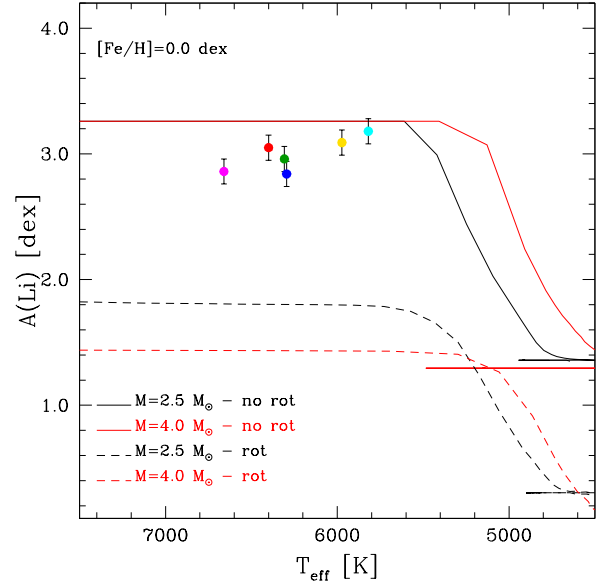


Fig. 4. Lithium abundances versus the effective temperatures compared with the predictions of the models STAREVOL (Lagarde et al. 2012). The curves are the predictions of the models for $2.5 M_{\odot}$ and $4.0 M_{\odot}$ with standard mixing (continuous lines) and with rotation-induced mixing and thermohaline instability (dashed lines).

Denissenkov, P. A. 1994, *A&A*, 287, 113
 Fitzpatrick, E. L. 1999, *PASP*, 111, 63
 Gaia Collaboration, Brown, A. G. A., Vallenari, A., et al. 2021, *A&A*, 649, A1
 Gaia Collaboration, Prusti, T., de Bruijne, J. H. J., et al. 2016, *A&A*, 595, A1
 Gray, D. F. 2008, *The Observation and Analysis of Stellar Photospheres*
 Grevesse, N., Asplund, M., Sauval, A. J., & Scott, P. 2010, *Ap&SS*, 328, 179
 Huang, W., Gies, D. R., & McSwain, M. V. 2010, *ApJ*, 722, 605
 Iben, Icko, J. 1967, *ARA&A*, 5, 571
 Kovtyukh, V., Lemasle, B., Chekhonadskikh, F., et al. 2016, *MNRAS*, 460, 2077
 Kovtyukh, V., Lemasle, B., Kniazev, A., et al. 2019, *MNRAS*, 488, 3211
 Kurucz, R. L. 1993, in *Astronomical Society of the Pacific Conference Series*, Vol. 44, IAU Colloq. 138: Peculiar versus Normal Phenomena in A-type and Related Stars, ed. M. M. Dworetzky, F. Castelli, & R. Faraggiana, 87
 Kurucz, R. L. & Avrett, E. H. 1981, *SAO Special Report*, 391
 Lagarde, N., Decressin, T., Charbonnel, C., et al. 2012, *A&A*, 543, A108
 Luck, R. E. & Lambert, D. L. 1992, *ApJS*, 79, 303
 Luck, R. E. & Lambert, D. L. 2011, *AJ*, 142, 136
 Lyubimkov, L. S., Lambert, D. L., Korotin, S. A., et al. 2011, *MNRAS*, 410, 1774
 Lyubimkov, L. S., Lambert, D. L., Korotin, S. A., Rachkovskaya, T. M., & Poklad, D. B. 2015, *MNRAS*, 446, 3447
 Maeder, A. & Meynet, G. 2000, *ARA&A*, 38, 143
 Ripepi, V., Catanzaro, G., Molinaro, R., et al. 2021, *MNRAS*, 508, 4047
 Romano, D., Magrini, L., Randich, S., et al. 2021, *A&A*, 653, A72
 Sasselov, D. D. 1986, *PASP*, 98, 561
 Simón-Díaz, S. & Herrero, A. 2014, *A&A*, 562, A135
 Takeda, Y., Kang, D. I., Han, I., Lee, B. C., & Kim, K. M. 2013, *MNRAS*, 432, 769
 Trentin, E., Ripepi, V., Catanzaro, G., et al. 2022, *MNRAS*
 Turner, D. G., Abdel-Sabour Abdel-Latif, M., & Berdnikov, L. N. 2006, *PASP*, 118, 410

Appendix A: Table and figures

Table A.1. Elemental abundances of OGLE-GD-CEP-0516, expressed in terms of the solar abundances (Grevesse et al. 2010), for 24 chemical species we measured in our target. Columns labelled with N represent the number of lines used in the analysis.

El	[El/H]	N	El	[El/H]	N
Li	2.03 ± 0.10	1	Cr	0.02 ± 0.05	5
C	-0.45 ± 0.05	3	Mn	-0.48 ± 0.51	5
O	-0.14 ± 0.16	2	Fe	-0.54 ± 0.16	169
Na	-0.04 ± 0.04	6	Co	0.35 ± 0.15	3
Mg	-0.40 ± 0.16	4	Ni	-0.32 ± 0.16	5
Al	0.02 ± 0.15	2	Cu	-0.18 ± 0.05	2
Si	0.18 ± 0.11	4	Zn	-0.33 ± 0.16	1
S	-0.17 ± 0.03	3	Y	-0.07 ± 0.04	4
Ca	-0.30 ± 0.11	9	Zr	0.24 ± 0.16	1
Sc	0.00 ± 0.04	5	Ba	-0.36 ± 0.12	4
Ti	-0.39 ± 0.21	20	La	0.17 ± 0.05	3
V	-0.02 ± 0.11	1	Nd	-0.41 ± 0.04	5

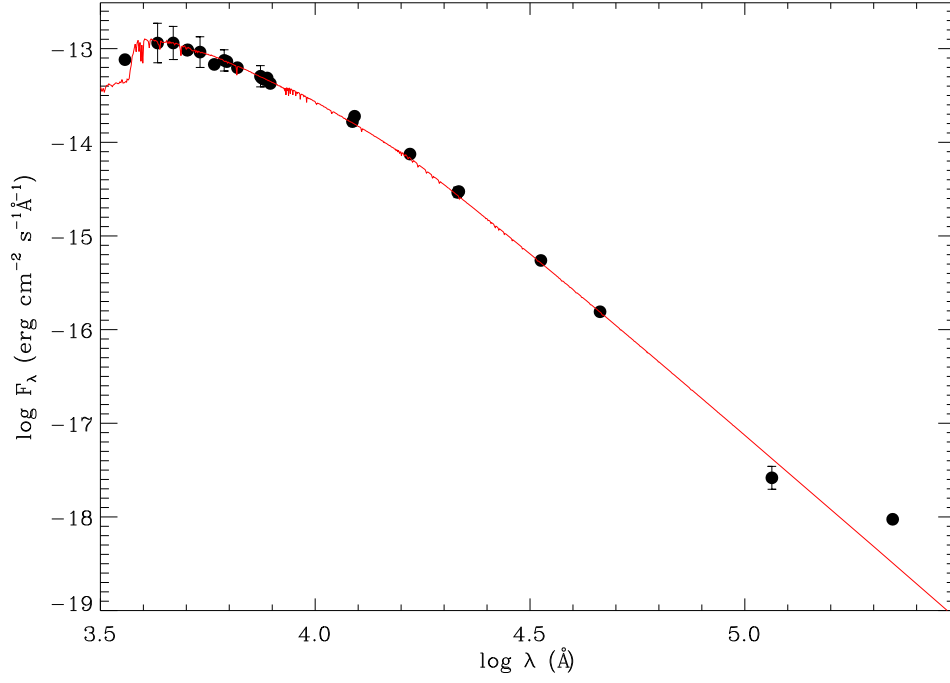


Fig. A.1. Spectral energy distribution of OGLE-GD-CEP-0516. Filled dots represent the observed fluxes as retrieved from the VOSA tool. A red line shows the theoretical flux computed using the ATLAS9 model for $T_{\text{eff}} = 6400$ K and $\log g = 1.5$.

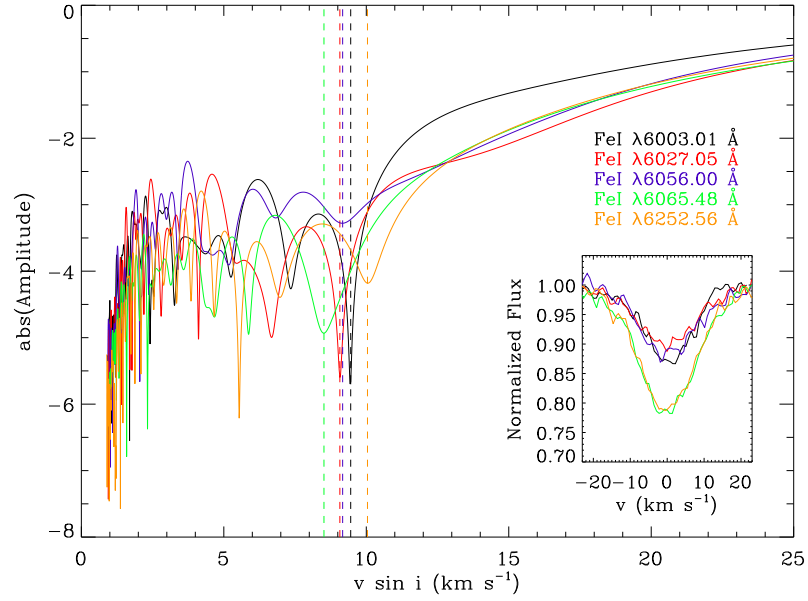


Fig. A.2. FFT of the Fe I $\lambda\lambda$ 6003.011, 6027.051, 6056.004, 6065.481, and 6252.555 Å. First zeroes of the FFT, i.e. the $v \sin i$ values, are indicated by vertical dashed lines. The inset shows the spectral line profiles.

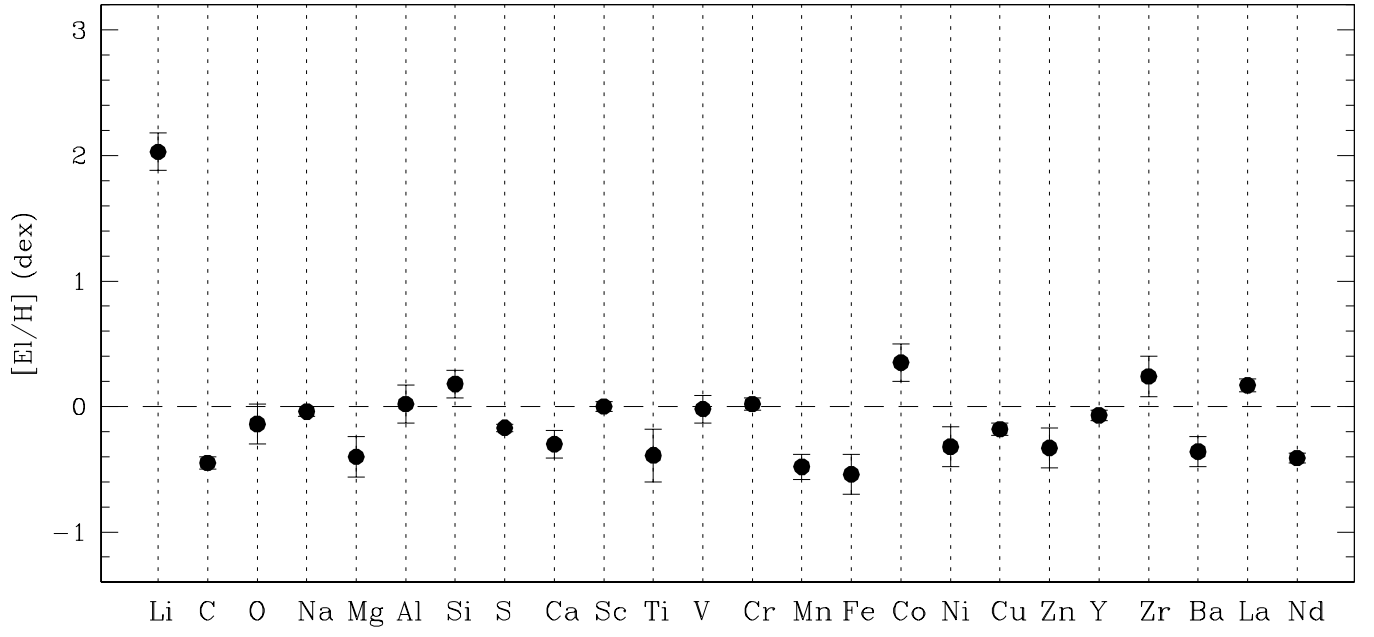


Fig. A.3. Chemical pattern derived for our target. The dashed line represents the solar standard abundance.